Preliminary Results of Experiments with Symmetric Baroclinic Instabilities[1]

P. H. STONE[2]

Division of Engineering & Applied Physics, Harvard University, Cambridge, Mass.

AND S. HESS, R. HADLOCK AND P. RAY

Dept. of Meteorology and Geophysical Fluid Dynamics Institute, Florida State University, Tallahassee

(Manuscript received 2 June 1969)

ABSTRACT

An experiment has been designed to test the predictions of nongeostrophic baroclinic stability theory. The apparatus is similar to the conventional rotating annulus experiments, except that the vertical temperature difference can be controlled as well as the horizontal temperature difference. Therefore, the Richardson number can be decreased by heating the bottom of the annulus relative to the top. The first qualitative observations derived from the experiment are described and are found to agree well with the theory. With no vertical temperature difference applied, the motion consists of a conventional baroclinic instability superimposed on the basic thermal wind. As the fluid is destabilized symmetric instabilities first appear superimposed on the baroclinic instability. As further destabilization occurs the symmetric instabilities completely replace the baroclinic instability, and are themselves subsequently replaced by small-scale, nonsymmetric instabilities.

1. Introduction

One of the simplest kinds of motion which can arise in the atmosphere of a rapidly rotating planet is a thermal wind oriented in the zonal (east-west) direction. Such a wind represents a balance between the Coriolis force and the latitudinal pressure gradient arising from differential solar heating (e.g., see Hess, 1959, p. 189). In fact, the prevailing winds in the earth's atmosphere when averaged over a long time are of just this kind. Since Jupiter, like the earth, is rapidly rotating and subject to differential solar heating, it seems likely that the predominantly zonal winds also observed in Jupiter's atmosphere (see Peek, 1958) are also basically thermal winds.

However, it is well known that thermal winds are unstable, and in the case of the earth's atmosphere the growing perturbations lead to the formation of cyclones and anticyclones (Eady, 1949). Recent analysis of the stability problem shows that there is more than one kind of perturbation which can grow, depending on the value of the Richardson number Ri (Stone, 1966), defined as

$$\mathrm{Ri}=\alpha g H^2\left(\frac{dT}{dz}-\Gamma\right)\Big/ u_0^2, \tag{1}$$

where g is the acceleration of gravity, H the vertical scale of the atmosphere, dT/dz the vertical temperature gradient, Γ the adiabatic lapse rate, u_0 the magnitude of the thermal wind, and α the expansion coefficient ($\alpha=1/T$ for a perfect gas). In particular, if $\mathrm{Ri}>0.95$, the kind of instability observed in the earth's atmosphere, baroclinic instability, dominates, but if $0.95>\mathrm{Ri}>0.25$, a different kind of instability, known as a symmetric instability, dominates. This latter type is called symmetric because the most rapidly growing perturbations have a structure which does not vary in the direction of the thermal wind. If $\mathrm{Ri}<0.25$, various other nonsymmetric instabilities dominate.

Since the visual observations of Jupiter indicate a very marked symmetry of the same kind (Peek, 1958), it is suggested that in Jupiter's atmosphere Ri lies in the range $0.95>\mathrm{Ri}>0.25$ and that the resulting symmetric instabilities cause the observed symmetry (Stone, 1967). This suggestion has gained added plausibility from a recent calculation which shows that the Reynolds stresses caused by these symmetric instabilities transport zonal momentum into equatorial regions (Gierasch and Stone, 1968). This is a possible mechanism for Jupiter's observed equatorial acceleration (Peek, 1958). Furthermore, the assumption that Ri is considerably smaller than in the earth's atmosphere, where $\mathrm{Ri}\sim 0.40$, is not unreasonable in view of the large heat flux from Jupiter itself reported by Low.[3] Such a flux would tend to destabilize the atmosphere and decrease Ri.

On the other hand, the theoretical ideas outlined above are based on calculations which make a number of assumptions and approximations which could be questioned when applying them to a real atmosphere. In particular, the stability analysis assumes infinitesimal

[1] Geophysical Fluid Dynamics Institute Contribution No. 8.
[2] Alfred P. Sloan Foundation Fellow.
[3] Low, F. J. 1969. Paper presented at the Third Arizona Conference on Planetary Atmospheres.

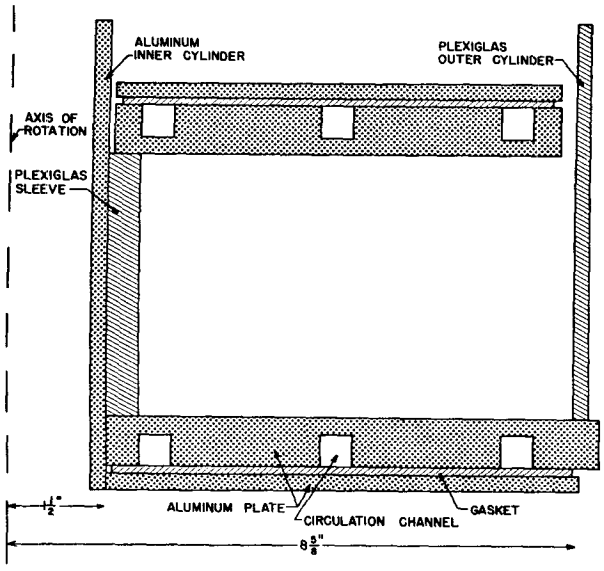

FIG. 1. Schematic cross section of the annulus.

perturbations, whereas in any quasi-steady state, finite-amplitude effects must in some sense be important. One way of investigating such effects is to produce finite-amplitude symmetric instabilities in a laboratory experiment.

In fact, many laboratory experiments have been carried out to study the stability of a thermal wind (e.g., see Fultz *et al.*, 1959, and Fowlis and Hide, 1965). However, in these experiments, only the horizontal temperature difference applied to the fluid is controlled. Since the resulting fluid motions have a considerable stabilizing effect on the temperature field, in these experiments Ri for the fluid is invariable greater than unity. Consequently, these experiments have had great success in studying baroclinic instabilities, but no symmetric instabilities have been observed.

In order to obtain different values of Ri in the laboratory, one must control the vertical temperature difference across the fluid as well as the horizontal difference. Then by making the lower boundary warmer than the top, the fluid will tend to be destabilized and smaller values of Ri should result. Therefore, we decided to construct an experiment like the conventional baroclinic instability experiments but with an additional provision for vertical heating. This paper reports the first qualitative observations from this experiment, which is being carried out at Florida State University.

2. Experimental apparatus

The fluid container consists of an annulus mounted on a rotating table. Thus, the annulus can be rotated about its central axis to simulate planetary rotation. Fig. 1 shows a vertical cross section through one-half of the annulus. The fluid is bounded above and below by aluminum plates, and on the inner and outer radii by plexiglas cylinders. Actually, in the earlier experiments, the inner plexiglas cylinder was absent and the inner boundary was an aluminum cylinder. The inner boundary of the fluid is at a radius of 3.8 cm if the inner plexiglas cylinder is absent, and of 5.1 cm if it is present; the outer boundary of the fluid is at a radius of 21.9 cm. Any depth of the fluid is possible up to 40.6 cm.

Channels have been machined in the aluminum plates and extend completely around the annulus. Fluid baths heated or cooled to various temperatures can be circulated through these channels to maintain the desired temperature boundary conditions. If the baths circulating through the outer channels are warmer than the baths in the inner channels, then we have a simulation of solar differential heating, with the outside of the annulus representing lower latitudes and the inside representing higher latitudes. In such an arrangement the radial direction is analogous to the meridional (north-south) direction in a planetary atmosphere; the azimuthal direction is analogous to the zonal direction; and the curvature of the planetary atmosphere is neglected. The thermal conductivity of the aluminum plates tends to smooth out the horizontal temperature gradient applied to the fluid. By making the temperatures of the baths in the lower channels different from those in the upper channels, we can simulate various degrees of heating from below in a planetary atmosphere. Thermocouples are located in each channel to measure the thermal boundary conditions being applied to the fluid. The temperature in the central channel of each plate was maintained at approximately the average temperature of the inner and outer channels. The plexiglas boundaries act essentially as thermal insulators.

The motion of the fluid can be viewed through the transparent plexiglas side of the annulus. The working fluid was a water solution of thymol blue, a pH indicator, titrated almost to the end point. Thus, the motions could be made visible by stringing wires through the fluid and sending a current through them (Baker, 1966). The ions formed at the wire change the pH sufficiently to change the color of the fluid, so a line of dye forms along the wire. Then the motion of the fluid past the wire sweeps the dye along with it, so that by following the dye the motions may be observed. Two or three wires, evenly spaced, were strung in the radial direction. Thus, by viewing the wires along the azimuthal direction, one can see the distribution of vertical motions along the meridional coordinate. The horizontal motions can also be seen by changing the viewing angle.

3. Description of the motions

The first experiments were carried out without the plexiglas inner cylinder, so the radial width of the fluid L was 18.1 cm. The fluid depth H was 8 cm, and the applied horizontal temperature difference Δ_h was 7.5K (positive meaning warmer on the outside). The period of rotation was 4 min, and the applied vertical tem-

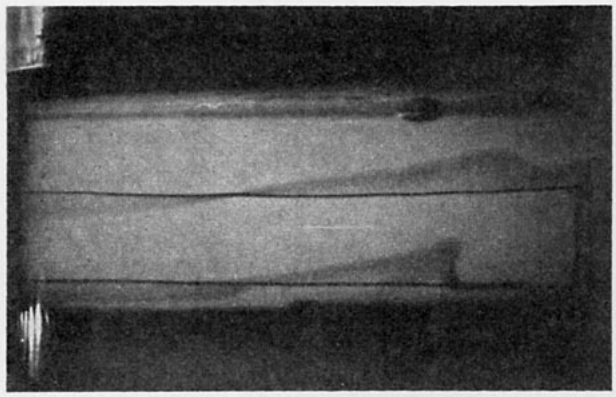

FIG. 2. Meridional distribution of vertical motions in a baroclinic instability, $\Delta_v \cong 0$K. In this and all subsequent figures the radius increases to the left.

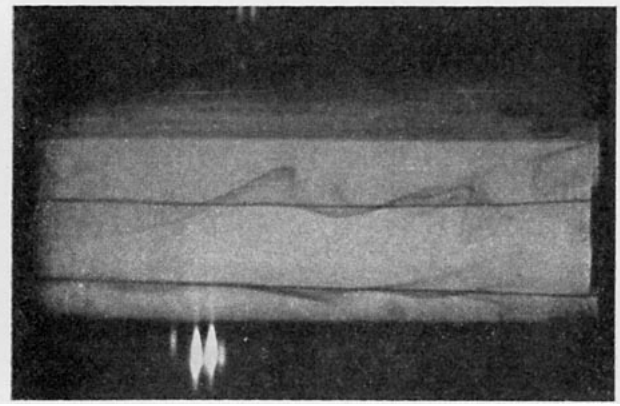

FIG. 4. The secondary instability fully developed, $\Delta_v \cong 1.5$K.

perature difference Δ_v was varied between -0.5 and 2K (positive meaning warmer at the bottom).

Fig. 2 illustrates the vertical motions present typically when $\Delta_v \lesssim 0$K. These motions are the kind typical of a baroclinic instability (Fultz *et al.*, 1959, p. 86). The dominant feature is that the motion is mainly indirect with sinking at the warm outside and rising at the cool inside. There is also a very narrow sinking region visible immediately adjacent to the inside cylinder. The dye has been coming off the wires long enough that the fast horizontal jet near the inner cylinder at the top wire has carried the dye part way around the cylinder and this jet is seen as a streak projected against the top of the inner cylinder.

Since the baroclinic instability is not symmetric, the vertical motions were not always as shown in Fig. 2, but the distribution shown is the one most commonly observed, and also is the distribution that one would obtain by averaging zonally (see Fultz *et al.*, 1959, p. 86). The meandering zonal jet typical of baroclinic instability was also easily seen in the experiment by looking down on the dye coming off of the wires.

Fig. 3 shows the typical vertical motions when $\Delta_v \cong 0.5$K. In the lower part of the fluid the motion is still that characteristic of a baroclinic instability, although the amplitude near the inner cylinder has increased considerably. However, in the upper part of the fluid it can be seen that a secondary instability, of smaller scale than the baroclinic instability, is now superimposed on the baroclinic instability. The motions for $\Delta_v = 0$–0.5K are approximately steady.

Fig. 4 illustrates the typical vertical motions when $\Delta_v \cong 1.5$K. Now the secondary instability has completely taken over from the baroclinic instability, and no trace of the latter remains. The vertical motions in the upper part of the fluid now show a set of meridional cells with a noticeable slant. On the original negative a total of six such cells are visible, extending all across the fluid, with the scale of the cells steadily decreasing towards the inner cylinder. On the prints only the cells in the middle are clearly visible. The motions are now not steady, but the pattern shown in Fig. 4 constantly reappears, with the instability apparently growing and then decaying repeatedly.

Fig. 5 shows another example of the secondary instability fully developed. This picture is from a different experimental run with the plexiglas inner cylinder now in place, so that $L = 16.8$ cm. The rotation period in this case was 2 min, and Δ_v was ~ 1.5K, but

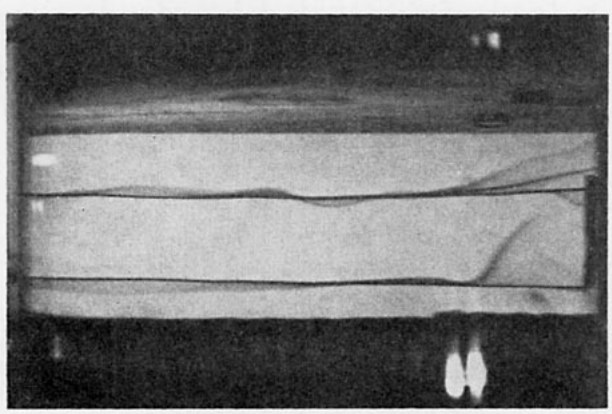

FIG. 3. Secondary instability superimposed on the baroclinic instability, $\Delta_v \cong 0.5$K.

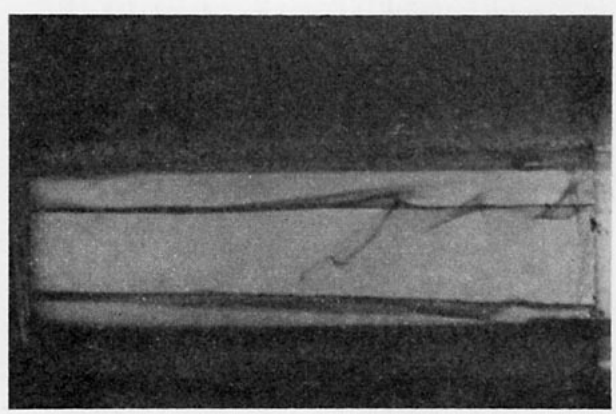

FIG. 5. Another example of the fully developed, secondary instability when the plexiglas inner cylinder is in place.

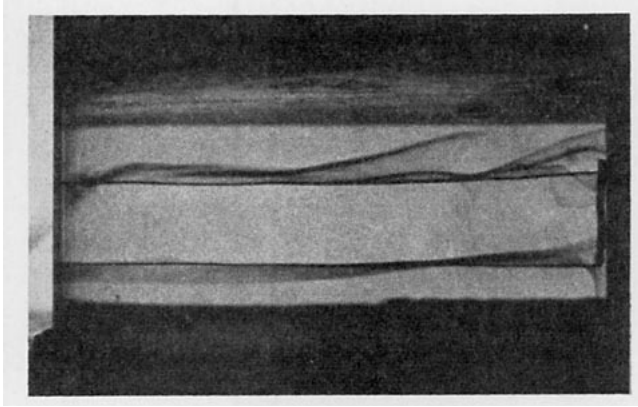

FIG. 6. Ridges superimposed on a baroclinic instability, $\Delta_v \cong 0.25$K.

otherwise the parameters were the same as for Figs. 2–4. In this case we again see very well-developed meridional cells with a pronounced slant, but now they appear near the inner cylinder in the upper part of the fluid. Note that the sinking motions in the outermost cell have actually turned around and started to rise again.

The most important question about this secondary instability is whether it is symmetric, i.e., independent of the downstream direction. One can determine this by letting the dye come off the wires for a period of time long enough so that the meridional cells are visible over a region extending substantially downstream from the wire. Within these experiments the meridional cells could be seen to be two dimensional, with their axes approximately parallel to the downstream flow. Illustrating this property in photographs is difficult, because the horizontal motion curves around the annulus and also has a significant radial component if the baroclinic instability is present. Consequently, any photograph taken after the dye has traveled downstream a significant distance and aimed at the same angle as Figs. 2–5 shows a superposition of the vertical motion at many different azimuth positions, all displaced relative to each other on the plane of the photograph. The best pictures of this kind can be taken when the amplitude of the secondary instability is small enough that the displacement of the dye particles above or below the wires is small even when they have traveled far downstream. Then by angling the camera to view the dye from above or below the horizontal plane containing the wires, one can get a photograph showing the downstream dependence reasonably well.

Fig. 6 shows one such picture taken when $\Delta_v \cong 0.25$K. The camera was placed low enough that it shows the vertical motions at the lower wire, but looks up through the dye sheet being carried downstream from the upper wire. The motion in the lower part of the fluid is clearly that associated with a baroclinic instability, but the dye sheet in the upper part of the fluid is seen at too great an angle for the vertical motions to be directly visible. Instead, a number of dark lines which are parallel to the downstream flow are visible in the upper dye sheet (in the figure the zonal structure is projected on the radial plane). These dark lines are caused by ridges in the upper dye sheet—specifically, they correspond to the side of the ridges which are tilted in the same direction as the line of sight. Although the ridges are parallel to the downstream flow, they make a moderately sharp angle with the radial wire because there is a substantial radial velocity component associated with the baroclinic instability already present. This component is directed inward in the upper part of the fluid at the particular azimuthal phase of the baroclinic instability illustrated in Fig. 2, 3 and 6 (cf. Fultz *et al.*, 1959, p. 86).

If one views the dye sheet coming off of the upper wire from the same direction as in Figs. 2–5, then one sees vertical motions just like those in the lower part of the fluid, i.e., the amplitude of the ridges is too small to see superimposed on the baroclinic wave. However, if Δ_v is increased, the ridges grow in amplitude until they form patterns like those seen in Figs. 3–5. Thus, it is clear that the ridges seen in Fig. 6 are in fact just the small amplitude form of the secondary instabilities seen in Figs. 3–5. Since the ridges are superimposed on the baroclinic instability, they rise and fall downstream as they pass through different phases of the baroclinic instability. On the original negative of Fig. 6 seven ridges can be counted. This would correspond to 13 or 14 meridional cells across the fluid. Since the photographs in Figs. 4 and 6 were taken under the same conditions, except for the value of Δ_v, it is apparent that the scale of the secondary instability increases as Δ_v increases.

Fig. 7 shows another example of the ridges, but this time viewed from above the horizontal plane of the upper wire. To make it possible to take a picture from this angle the depth of the fluid was increased to 16 cm. This photograph illustrates particularly well the two-dimensionality of the secondary instability. Note that the plexiglas inner cylinder is present in this case.

Finally, if Δ_v is increased to about 1.75K or more, nonsymmetric, small-scale instabilities set in. The motion is even less steady and no overall organization is apparent.

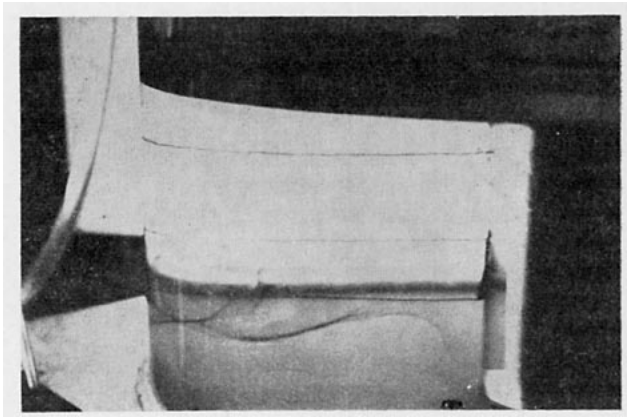

FIG. 7. Another example of ridges.

4. Comparison with theory

Qualitatively the observations described above agree well with the predictions of the stability theory. As the fluid is destabilized, the baroclinic instability is gradually replaced by an instability which has the right kind of symmetry and vertical slant to be a symmetric instability (Stone, 1966). This instability is in turn replaced by nonsymmetric instabilities when the destabilization is continued. However, it is also possible to estimate various parameters and obtain some more quantitative checks with the theory.

The theory (Eady, 1949; Stone, 1966) is based on the assumptions that the motion is inviscid and in hydrostatic equilibrium. Therefore, before making a more detailed comparison between theory and observation, we will check whether these assumptions are valid for our experiment. Frictional effects can be estimated by calculating the Taylor number Ta, defined as

$$\mathrm{Ta}=\frac{4\Omega^2H^4}{\nu^2}, \tag{2}$$

where ν is the kinematic viscosity of the fluid. Since $\nu=10^{-2}$ cm^2 sec^{-1} for water, Ta for the experiment illustrated in Figs. 2, 3, 4 and 6 is 1.1×10^5. This is large enough that frictional effects on the instabilities will be small. The horizontal boundary layers are about 1/20 the depth of the fluid.

It is interesting to note that at these values of Ta baroclinic instabilities do not occur in the conventional experiments (Fultz *et al.*, 1959; Fowlis and Hide, 1965) although they do in ours. This is probably due to the fact that we had to supply more heat to the lower boundary than in the conventional experiments in order to make $\Delta_v=0$. As a result, we probably have smaller values of Ri than in the conventional experiments where $\Delta_v<0$, and this would increase the baroclinic instability (Stone, 1966). Such a supposition is borne out by the observation that the secondary instabilities first appear for the very small value $\Delta_v\cong0.25$K, and theory predicts that this should correspond to Ri$=1$. Since $\Delta_h=7.5$K, it is unlikely that $\Delta_v=0$ will correspond to much larger values of Ri.

In checking the assumption of hydrostatic equilibrium we first define

$$\epsilon=\frac{w/t}{\alpha g\Delta_v}, \tag{3}$$

where w is the magnitude of the vertical velocity and t the time scale. Therefore, ϵ is the ratio of the vertical accelerations to the buoyancy force, and $\epsilon\ll1$ will insure hydrostatic equilibrium. For symmetric instabilities $t=(2\Omega)^{-1}$, where Ω is the angular rate of rotation, and $w=(H/L)u_0$ (see Stone, 1966). From the thermal wind relation,

$$2\Omega\frac{\partial u}{\partial z}=\alpha g\frac{\partial T}{\partial y}, \tag{4}$$

we can estimate that

$$u_0=\frac{\alpha gH\Delta_h}{2\Omega L}. \tag{5}$$

Substituting for w, t and u_0 into Eq. (3), we obtain

$$\epsilon=\frac{H^2}{L^2}\frac{\Delta_h}{\Delta_v}. \tag{6}$$

In general, the values of Δ_h and Δ_v across the interior of the fluid (not including the boundary layers) are different from the values applied at the boundaries because of the stabilizing influence of the motions. However, it is these interior values which are relevant in estimating quantities such as ϵ and Ri since the instabilities occur in the interior. If the total temperature contrast applied to the boundaries is Δ, then

$$\Delta_h+\Delta_v=\Delta. \tag{7}$$

This same relation also holds for the interior values, Δ_h' and Δ_v', since the motion cannot destroy isotherms. It is these values that we will use in calculating ϵ. However, their ratio will be changed from that for the applied values. If s is the magnitude of the slope of the isotherms in the interior of the fluid, we have

$$s=\left(\frac{dz}{dy}\right)_T=\frac{H}{L}\frac{\Delta_h'}{\Delta_v'}. \tag{8}$$

Thus, if we know s we can calculate ϵ directly, and from Eqs. (7) and (8), we can calculate the interior values of Δ_h' and Δ_v'.

The theory assuming hydrostatic equilibrium predicts that the motions of the most unstable symmetric perturbations will have meridional cells which have a vertical slant parallel to the isotherms (Stone, 1966). More recent calculations which will be published separately (Stone[4]) show that the vertical slope of the most unstable perturbations is always greater than the slope of the isotherms if the assumption of hydrostatic equilibrium is relaxed. Consequently, we can get an upper bound on s and ϵ by measuring the vertical slope of the meridional motions in the photographs. For example, from Fig. 4, we measure slopes ranging from 0.25–0.45. If we take 0.35 as typical, then we have $s\leq0.35$. Since H and L for this photograph were 8 and 18.1 cm, respectively, we can calculate that $\epsilon=(H/L)s\leq0.15$. Therefore, hydrostatic equilibrium is a good first approximation, and we can in fact consistently equate the slope of the meridional motions to the slope of the isotherms.

[4] Stone, P. H., 1969: The effects of diffusion and non-hydrostatic equilibrium on asymmetric baroclinic instabilities (in preparation).

Now we can use these measured slopes to calculate values of Ri and see if they are consistent with the inviscid, hydrostatic theory. For a liquid $\Gamma=0$, and if we substitute Eq. (5) into Eq. (1) and approximate dT/dz by finite differences, we obtain

$$\mathrm{Ri}=\frac{4\Omega^2L^2\Delta_v'}{\alpha g H\Delta_h'^2}. \tag{9}$$

Using Eqs. (7) and (8) to replace Δ_v' and Δ_h' by Δ and s, we obtain

$$\mathrm{Ri}=\frac{4\Omega^2(H+sL)}{\alpha g\Delta s^2}. \tag{10}$$

Now we calculate Ri for the conditions illustrated in Fig. 4 by again using the value $s=0.35$. For water $\alpha=2\times10^{-4}(^\circ\mathrm{K})^{-1}$ and the conditions in Fig. 4 corresponded to $\Delta=9\mathrm{K}$ and a period of rotation of 4 min. Thus, we calculate $\mathrm{Ri}=0.2$.

We can perform similar calculations for Fig. 5. In this case the measured slopes range from 0.8 to 0.4 and we will take $s=0.6$ as typical. We then find $T=4\times10^5$, $\epsilon=0.3$, $\mathrm{Ri}=0.3$. Since the situations depicted in Figs. 4 and 5 are ones for which the vertical heating is almost but not quite strong enough to cause a changeover from the symmetric to the nonsymmetric instabilities, and since the theory predicts that the changeover should occur for $\mathrm{Ri}=0.25$ (Stone, 1966), the agreement between the calculated and theoretical values is quite good. Unfortunately, the smaller amplitude symmetric instabilities are too small to show their slope, so we cannot check the upper limit on Ri.

We can also calculate the Rossby numbers for Figs. 4 and 5. By definition

$$\mathrm{Ro}=\frac{u_0}{2\Omega L}, \tag{11}$$

and substituting for u_0 from (5), we find that we can express Ro simply in terms of Ri, i.e.,

$$\mathrm{Ro}=\frac{H}{sL\mathrm{Ri}}. \tag{12}$$

We thus find that $\mathrm{Ro}=6$ for Fig. 4 and $\mathrm{Ro}=3$ for Fig. 5.

Finally, we can make one more check. Theory predicts that the most unstable horizontal wavelengths for the symmetric instabilities are those which are small compared with the cut-off wavelength, i.e.,

$$L_0=2L\mathrm{Ro}\sqrt{1-\mathrm{Ri}}. \tag{13}$$

Using the same numbers as above we calculate that $L_0=190$ cm for Fig. 4 and 80 cm for Fig. 5. Since the motions in these photographs have wavelengths of about 6 and 3 cm, respectively, we again have agreement with theory. Probably the very shortest wavelengths are stabilized by the frictional effects omitted in the theory.

5. Conclusions

The qualitative observations described above appear to verify substantially the predictions of stability theory. This conclusion should be regarded as tentative until more detailed and quantitative measurements of the motions and temperature field become available. The experimental apparatus is now being modified so that such measurements can be made.

However, taking the qualitative observations at their face value one can conclude that finite-amplitude effects do not qualitatively modify the essential properties of the motions predicted by the small-amplitude stability theory. This removes one difficulty in applying the theory to Jupiter's atmosphere. However, other difficulties remain, and perhaps the most important one is the failure of the theory (and also of the experiment) to include curvature effects. Since Jupiter's primary zonal current is located in equatorial regions, curvature effects could be important.

Acknowledgments. This research has been supported by the National Aeronautics and Space Administration under Grant NsG-173-63/10-004-003 and in part by the Office of Naval Research under Contract N-00014-68-A-0159.

REFERENCES

Baker, D. J., 1966: A technique for the precise measurement of small fluid velocities. *J. Fluid Mech.*, **26**, 573–575.

Eady, E. T., 1949: Long waves and cyclone waves. *Tellus*, **1**, No. 3, 33–52.

Fowlis, W. W., and R. Hide, 1965: Thermal convection in a rotating annulus. *J. Atmos. Sci.*, **22**, 541–558.

Fultz, D., R. R. Long, G. V. Owens, W. Bohan, R. Kaylor and J. Weil, 1959: Studies of thermal convection in a rotating cylinder. *Meteor. Monogr.*, **4**, No. 21, 1–104.

Gierasch, P. J., and P. H. Stone, 1968: A mechanism for Jupiter's equatorial acceleration. *J. Atmos. Sci.*, **25**, 1169–1170.

Hess, S. L., 1959: *Introduction to Theoretical Meteorology*. New York, Holt, Rinehart and Winston, 362 pp.

Peek, B. M., 1958: *The Planet Jupiter*. London, Faber and Faber, 283 pp.

Stone, P. H. 1966: On non-geostrophic baroclinic stability. *J. Atmos. Sci.*, **23**, 390–400.

——, 1967: An application of baroclinic stability theory to the dynamics of the Jovian atmosphere. *J. Atmos. Sci.*, **24**, 642–652.